CsCu$_5$Se$_3$: A Copper-Rich Ternary Chalcogenide Semiconductor with Nearly Direct Band Gap for Photovoltaic Application

Zhiguo Xia,*,†,△ Huajing Fang,‡,△ Xiuwen Zhang,*,§ Maxim S. Molokeev,⊥,¶,‖ Romain Gautier,# Qingfeng Yan,‡ Su-Huai Wei,□ and Kenneth R. Poeppelmeier*,○

†The Beijing Municipal Key Laboratory of New Energy Materials and Technologies, School of Materials Sciences and Engineering, University of Science and Technology Beijing, Beijing 100083, China

‡Department of Chemistry, Tsinghua University, Beijing 100084, China

§College of Electronic Science and Technology, Shenzhen University, Guangdong 518060, China

⊥Laboratory of Crystal Physics, Kirensky Institute of Physics, Federal Research Center KSC SB RAS, Krasnoyarsk 660036, Russia

¶Department of Physics, Far Eastern State Transport University, Khabarovsk 680021, Russia

‖Siberian Federal University, Krasnoyarsk 660041, Russia

#Institut des Matériaux Jean Rouxel (IMN), Université de Nantes, CNRS, 2 rue de la Houssinière, BP 32229, Nantes, Cedex 03 44322, France

□Beijing Computational Science Research Center, Beijing 100094, China

○Department of Chemistry, Northwestern University, 2145 Sheridan Road, Evanston, Illinois 60208-3113, United States

S *Supporting Information*

ABSTRACT: Discovery of new semiconductor candidates with suitable band gaps is a challenge for optoelectronic application. A facile solvothermal synthesis of a new ternary chalcogenide semiconductor CsCu$_5$Se$_3$ is reported. The telluride CsCu$_5$Te$_3$ is also predicted to be stable. CsCu$_5$Se$_3$ is isostructural with CsCu$_5$S$_3$ (space group *Pmma*). The band gap calculations of these chalcogenide semiconductors using hybrid density functional theory indicate nearly direct band gaps, and their values (about 1.4 eV) were confirmed by the optical absorption spectroscopy. These alkali metal copper chalcogenides are interesting examples of copper-rich structures which are commonly associated with favorable photovoltaic application.
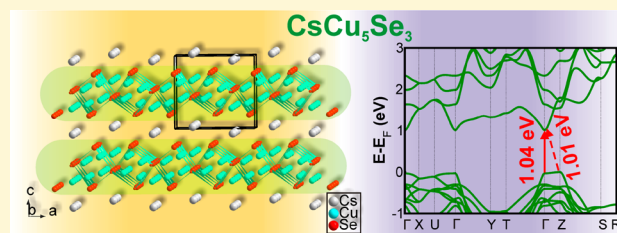
INTRODUCTION

Laboratory discovery of never before made compounds offers opportunities for fundamental studies of technologically relevant functionalities.[1−4] Among different families of functional materials, semiconductors with energy band gaps (E_g) around 1.3−1.5 eV are essential for solar energy conversion.[5] For example, elemental Si and binary GaAs, both well-known, have suitable band gaps for photovoltaic applications.[6] Nonetheless, these materials continue to motivate the search for more efficient optoelectronic materials and devices. In this context, various copper-based chalcogenides have recently been in the focus of interest. This group of materials consists of a relatively large number of binary, ternary, and multinary phases.[7−9] In particular, some copper-based I-I-VI group compounds have been predicted to be stable using density functional-based first-principles thermodynamics.[10] Using these predictions, the new RbCuTe phase could be prepared revealing a new type of strain-tolerant inorganic material,[11] which further inspired us to study other new I-I-VI group copper chalcogenides.[12]

Solution-based synthetic approaches such as the solvothermal route can provide not only totally different reaction and thermo-chemical pathways compared to solid-state reactions but also convenient, soft-chemistry processes capable of creation of targeted materials with desirable shapes, sizes, and compositions.[13,14] For alkali metal−copper chalcogenides, only a few examples such as NaCu$_5$S$_3$ or KCu$_7$S$_4$ have been prepared under hydrothermal conditions.[15,16]

In this study, a combined theory and experimental investigation was undertaken to discover new I-I-VI group copper chalcogenides A-Cu-X (A = Li, Na, K, Rb, and Cs; X = S, Se, and Te) and the new compound CsCu$_5$Se$_3$ isostructural to CsCu$_5$S$_3$ was isolated. We further present calculations of the three chalcogenides CsCu$_5$X$_3$ (X = S, Se, Te) to obtain preliminary evaluation of their optical properties. This work illustrates how solution-based methods can target specific

phases and compositions that are not readily prepared by solid state reaction.

EXPERIMENTAL SECTION

Materials and Preparation. All chemicals are available commercially and were used without further purification: CsOH·H$_2$O (99.5%, Alfa Aesar), Cu$_2$S (99.5%, Alfa Aesar), Cu$_2$Se (99.5%, Alfa Aesar), Thiourea (99%+, Sigma-Aldrich), diphenyl diselenide (98%+, Sigma-Aldrich), and ethanediamine (≥99%, Sigma-Aldrich). CsCu$_5$S$_3$ and CsCu$_5$Se$_3$ microcrystals were synthesized by the solvothermal method with ethanediamine as solvent. In a typical procedure implemented for the synthesis of CsCu$_5$Se$_3$, 3.125 mmol Cu$_2$Se, 0.625 mmol diphenyl diselenide, 12.5 mmol CsOH·H$_2$O (10-fold excessive stoichiometry), and 6 mL of ethanediamine were added in a 3 × 1.75 in. rectangle Teflon pouch that was made and sealed as previously described.[17] Then, six Teflon pouches were placed in a 100 mL Teflon-lined Parr pressure vessel filled with 50 mL of deionized H$_2$O as backfill. Pressure vessels were heated to 200 °C for 24 h and cooled to room temperature naturally. Pouches were opened in air, and the microcrystals were recovered via vacuum filtration and followed by drying in a vacuum furnace at 60 °C for 12 h. CsCu$_5$Se$_3$ microcrystals can also be prepared using this process with relatively big amounts (several grams every batch depending on the volume of the pouches used).

Characterization. Phase purity and crystal structure of the as-prepared powders were characterized by powder X-ray diffraction using Rigaku MiniFlex 600 diffractometer with the Cu Kα source, operating at 40 kV and 15 mA. The morphology of powders was observed by scanning electron microscopy (SEM, JEOL JSM-6510). The powders were further characterized with high-resolution transmission electron microscopy (HRTEM) and energy-dispersive X-ray spectroscopy (EDX) by JEM 2100F. The X-ray photoelectron spectroscopy (XPS) experiments were performed on CsCu$_5$X$_3$ powders using PHI Quantera SXM spectrometer. Thermogravimetric analysis was performed using a thermobalance equipped with a differential thermal analyzer (Setaram Labsys Evo). To measure the energy band gap, UV−vis spectra of these semiconductors were collected on a SHIMADZU UV-3600 spectrometer.

Computational Methods. The total energy and band structure of Cs-Cu-X (X = S, Se, Te) were calculated by density functional theory (DFT)[18] using the projector-augmented wave (PAW) pseudopotentials[19] with the exchange-correlation of Perdew−Burke−Ernzerhof (PBE) form[20] as implemented in the Vienna ab Initio Simulation Package (VASP[21]). We chose the energy cutoff of 350 eV and reciprocal space grids with densities of about $2\pi \times 0.03$ Å^{-1}. The initial crystal structure was taken from experiment, and the lattice constants as well as atomic positions were fully relaxed under a tolerance of 10^{-5} eV per unit cell.[22] To overcome the DFT band gap problem, we employed a hybrid functional (HSE06) to correct the band gap.[23]

RESULTS AND DISCUSSION

Crystallography and Structural Aspects. In the XRD patterns, all the peaks recorded for the as-prepared CsCu$_5$S$_3$ and CsCu$_5$Se$_3$ phases were indexed using the previous reported structural model of CsCu$_5$S$_3$.[24] The powder diffraction data of the as-prepared CsCu$_5$S$_3$ and CsCu$_5$Se$_3$ phases were further analyzed by Rietveld refinement (Figures 1a and b). The crystal structure parameters and details of the refinement as well as the fractional atomic coordinates and isotropic displacement parameters are listed in Tables 1 and 2. The crystallographic information files (CIF) of CsCu$_5$S$_3$ and CsCu$_5$Se$_3$ are presented in the Supporting Information. The insets of Figures 1a and b show the representative crystal structure with the same space group *Pmma*. Both CsCu$_5$X$_3$ (X = S, Se) exhibit a layered structure, as shown in Figure 1c. Cesium ions are located between the adjacent CuX$_3$ (X = S, Se) layers. Cell parameters are shown to increase unequally when replacing S by Se: $\delta_a =$
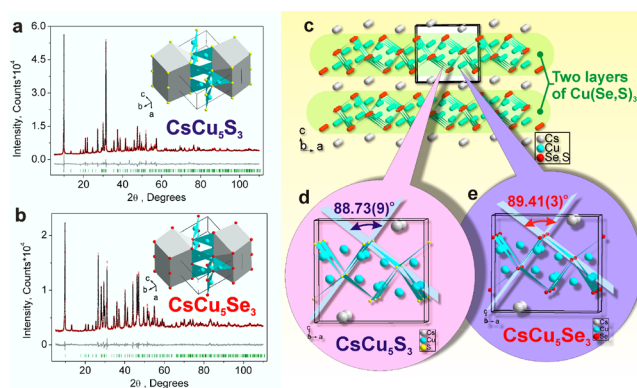
Figure 1. Crystal structure and Rietveld refinement profiles of (a) CsCu$_5$S$_3$ and (b) CsCu$_5$Se$_3$. (c) Layered structure diagram of CsCu$_5$X$_3$. (d and e) Contrast of the fine structures with different anions for the two compounds.

**Table 1. Main Parameters of Processing and Refinement of CsCu$_5$X$_3$ (X = S, Se)**

compound	CsCu$_5$S$_3$	CsCu$_5$Se$_3$
space group	*Pmma*	*Pmma*
a, Å	9.6365 (3)	9.9909 (3)
b, Å	3.9547 (2)	4.0978 (1)
c, Å	8.9490 (2)	9.0071 (3)
V, Å^3	341.04 (2)	368.76 (2)
Z	2	2
k	5−110	5−110
R_{wp}, %	3.98	2.39
R_p, %	2.68	1.78
R_{exp}, %	1.51	1.62
χ^2	2.64	1.47
R_B, %	2.36	0.57

Table 2. Fractional Atomic Coordinates and Isotropic Displacement Parameters (Å^2) of CsCu$_5$X$_3$ (X = S, Se)

|	x	y	z	B_{iso}	occ.
			CsCu$_5$S$_3$		
Cs	0.25	0	0.0563 (2)	2.6 (2)	1
Cu1	0.1165 (3)	0.5	0.4198 (2)	2.3 (2)	1
Cu2	0.0755 (3)	0	0.6501 (3)	3.0 (2)	1
Cu3	0.25	0.5	0.7108 (3)	2.5 (2)	1
S1	0.25	0	0.4558 (6)	2.0 (2)	1
S2	0.0273 (6)	0.5	0.7774 (4)	2.0 (2)	1
			CsCu$_5$Se$_3$		
Cs	0.25	0	0.0473 (2)	2.8 (2)	1
Cu1	0.1090 (2)	0.5	0.4299 (3)	3.8 (2)	1
Cu2	0.0749 (2)	0	0.6416 (3)	2.5 (2)	1
Cu3	0.25	0.5	0.6872 (3)	2.4 (2)	1
Se1	0.25	0	0.4527 (3)	2.0 (2)	1
Se2	0.0304 (2)	0.5	0.7822 (2)	2.0 (2)	1

3.68%, δ_b = 3.62%, δ_c = 0.65%. The increased angle between planes passing through CuX$_3$ triangles (Figures 1d and e) is responsible for the difference between δ_a and δ_c.

Morphology and Elemental Analyses. We analyzed the morphology of the as-synthesized CsCu$_5$X$_3$ powders. The SEM images in Figures 2a and b show typical one-dimensional micro/nanorod structure of the compounds, which is a robust indicator of excellent crystallinity of the compound, as it was reported on for several other chalcogenides crystals.[25,26] Under
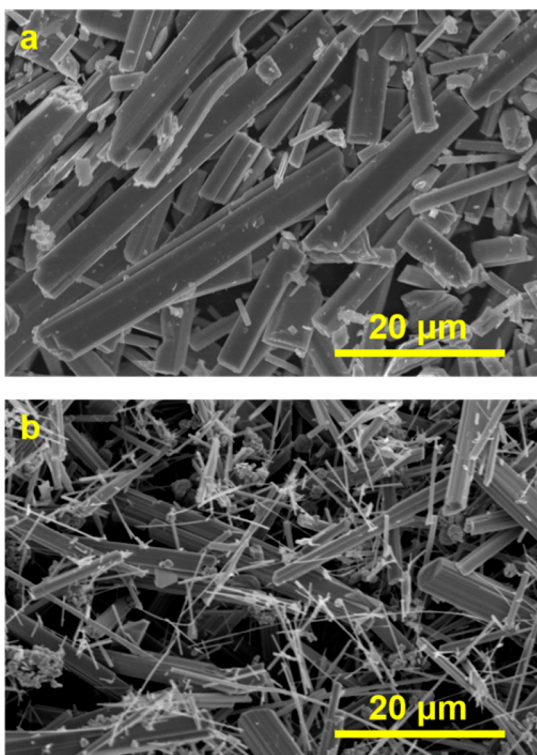
Figure 2. SEM images of the as synthesized (a) CsCu$_5$S$_3$ and (b) CsCu$_5$Se$_3$.

the same reaction conditions, CsCu$_5$S$_3$ microcrystals grow to larger size in comparison to that of CsCu$_5$Se$_3$. To provide more details, we studied the microstructure and crystallinity of the individual nanorods. As shown in Figure 3a, the energy dispersive X-ray (EDX) mapping of a single CsCu$_5$S$_3$ nanorod reveals that Cs, Cu, and S elements are uniformly distributed over the nanorod. The EDX spectrum (see Figure S1a) further reveals that the atomic percent ratio of Cs:Cu:S is close to the stoichiometry (1:5:3). A high-resolution transmission electron
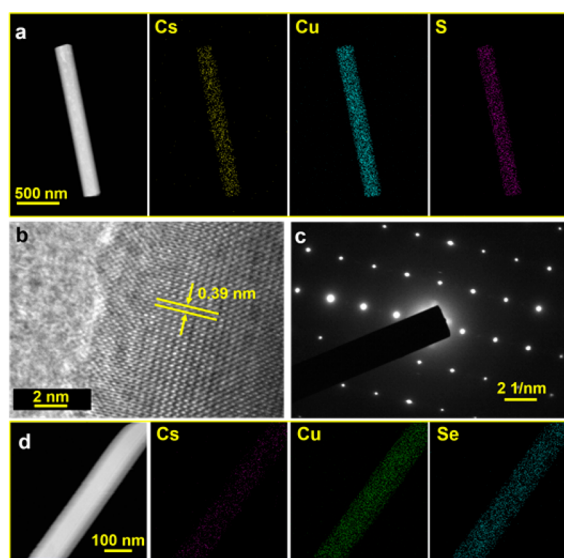
Figure 3. (a) TEM-EDX mapping of a single CsCu$_5$S$_3$ nanorod. (b) HRTEM image and (c) corresponding SAED pattern of the CsCu$_5$S$_3$ nanorod. (d) TEM-EDX mapping of a single CsCu$_5$Se$_3$ nanorod.

microscopy (HRTEM) image at the edge of the CsCu$_5$S$_3$ nanorod is shown in Figure 3b. The well-resolved lattice fringes with interplanar distance of 0.39 nm were observed. The selective area electron diffraction (SAED) pattern (see Figure 3c) exhibits several bright spots, confirming the well-defined single crystalline state of the entire CsCu$_5$S$_3$ nanorod. As a comparison, the EDX mapping of a single CsCu$_5$Se$_3$ nanorod can be found in Figure 3d. The atomic percent ratio of this ternary semiconductor is also close to its stoichiometry (EDX spectrum in Figure S1b). X-ray photoelectron spectroscopy (XPS) was employed to further analyze the surface chemical composition. Figure 4 shows the high-resolution XPS spectra of
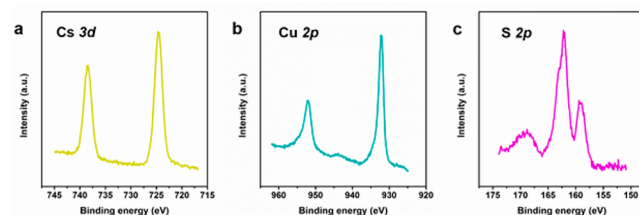
Figure 4. X-ray photoelectron spectra of (a) Cs 3d, (b) Cu 2p, and (c) S 2p in the as synthesized CsCu$_5$S$_3$ powder.

Cs 3d, Cu 2p and S 2p orbitals in CsCu$_5$S$_3$. In particular, the 2 distinct peaks located at 952.1 and 932.2 eV can be assigned as the binding energy of Cu 2p$_{1/2}$ and Cu 2p$_{3/2}$, in agreement with the Cu−S framework contained in the aforementioned layered structure.[27,28] Besides the Cu 2p doublet, the binding energy of S 2p components could be compared with the values reported for other sulfides, and a survey can be found elsewhere.[29]

Thermal Stability. Thermogravimetric analysis (TGA) and differential thermal analysis (DTA) were employed to assess the thermal stability of both compounds. TGA curves shown in Figures 5a and b indicate that both CsCu$_5$S$_3$ and CsCu$_5$Se$_3$ were thermally stable up to 500 °C. Even heating to a considerably higher temperature (up to 800 °C) resulted in a percentage of weight loss of still less than 1%. The DTA
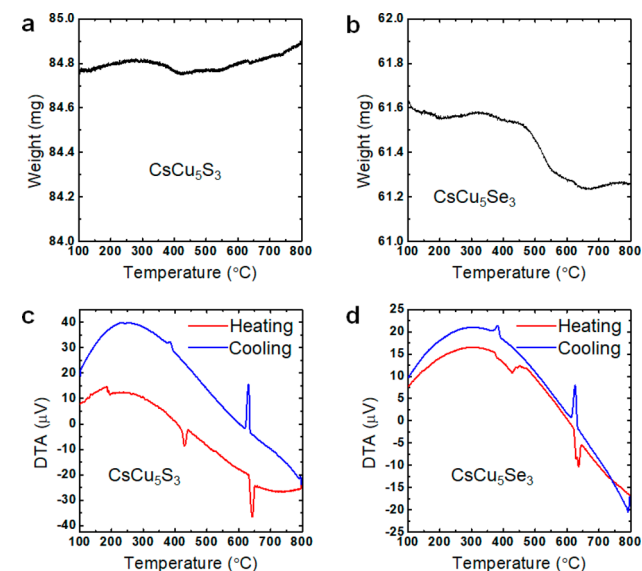
Figure 5. Thermogravimetric curves of the two ternary chalcogenide semiconductors (a) CsCu$_5$S$_3$ and (b) CsCu$_5$Se$_3$. Differential thermal analyses of (c) CsCu$_5$S$_3$ and (d) CsCu$_5$Se$_3$.

performed on the ground crystals indicated that there are two endothermic peaks with increasing temperature, and the first one at about 400 °C may be the decomposition of the remained organic ligands, while the second one at about 650 °C should be the structural phase transition temperature.[21] It is reported that at 582 °C the orthorhombic modification of $CsCu_5S_3$ transforms easily into the tetragonal one, while the reverse reaction occurs very slowly, so that we can find the hysteretic exothermic peak during the decreasing temperature. Because $CsCu_5Se_3$ is iso-structural with $CsCu_5S_3$, the similar structural phase transition can be expected, as shown in Figures 5c and d. These results confirm that the novel ternary chalcogenide semiconductors possess excellent thermal stability.

Semiconductor Properties. The optical properties of $CsCu_5S_3$ and $CsCu_5Se_3$ were investigated. The general method described in ref 30 was used to determine the energy band gaps for considering the effects of internal carriers and energy broadening on the measured optical spectrum. Figure 6a
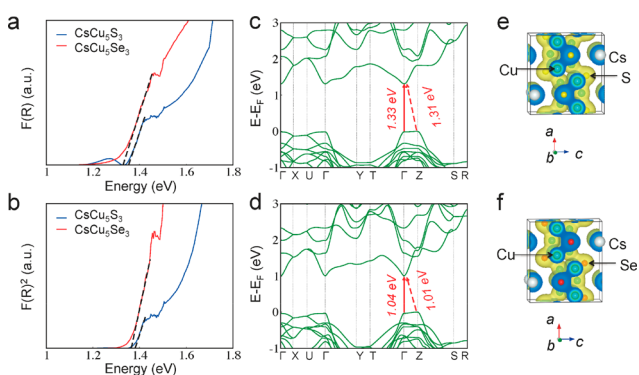

Figure 6. Absorbance ($\alpha = F(R)$) (a) and $F(R)^2$ plots (b) of $CsCu_5X_3$ (X = S, Se). Electronic band structures from DFT with band gap corrected by HSE06 of $CsCu_5S_3$ (c) and $CsCu_5Se_3$ (d). Charge density from DFT for $CsCu_5S_3$ (e) and $CsCu_5Se_3$ (f).

describes the relationship between absorbance (given by $\alpha = F(R) = (1 - R)^2/(2R)$, where R is the reflectance)[26] and photon energy $h\nu$. Figure 6b plots the relationship between $F(R)^2$ and photon energy $h\nu$. The energy band gaps (E_g) of the ternary chalcogenides were deduced from the extrapolated x-intercepts given by $E(F)$ and $E(F^2)$ of $F(R)$ vs $h\nu$ and $F(R)^2$ vs $h\nu$ plots, respectively: $E_g = 2E(F^2) - E(F)$. The non-negligible difference between $E(F)$ and $E(F^2)$ indicates the considerable effects of energy broadening and carriers in the materials at experimental conditions. Energy band gaps of the $CsCu_5S_3$ and $CsCu_5Se_3$ were found to be ~1.41 and ~1.40 eV, respectively. These values are very close to the band gap of GaAs, one of the best photovoltaic materials up to now,[31] and they are smaller than the band gap (1.93 eV) of PV absorber Cu_2O, whose efficiency is limited by adjacent materials in devices as well as wide band gap.[32]

In addition to experimental analyses of the two ternary semiconductors, $CsCu_5S_3$ and $CsCu_5Se_3$, theoretical investigations via electronic structure calculations were performed to better understand the nature of the physical properties. The band gaps of $CsCu_5X_3$ (X = S, Se) were calculated using hybrid density functional theory (HSE06).[23] Detailed band structures were obtained from DFT with band gaps corrected by HSE06. The results show that the band gap of $CsCu_5S_3$ is close to the optimum value for photovoltaic absorbers (Figure 6c). The

indirect band gap is very close to the direct band gap (corresponding to the measured optical gap), as indicated by the red arrows (e.g., differ by 14 meV for $CsCu_5S_3$). The indirect gap is from the valence band maximum (VBM) (Cu d and S p states) at Z point to the conduction band minimum (CBM) (Cu s, Cu d, and S p states) at Γ point. After optical absorption, most of the holes relax into the Z valley with a small portion into the Γ valley due to thermal distribution of carriers and electrons relaxing into the Γ valley; thus, the radiative recombination between electron and hole is significantly suppressed, with a very small energy cost (e.g., 14 meV for $CsCu_5S_3$). In ref 26, the thermal distribution of the holes in this type of indirect-gap semiconductor (labeled as OT3 in ref 27) is described by the factor $f_r = e^{-\Delta/kT}$, where k is the Boltzmann constant and T is the temperature. According to Yu et al.,[33] the smaller the Δ, the larger the f_r, and the better for PV absorber. The energy waste is associated with the energy range $E_g \sim E_g + \Delta$; here, the optical transition is forbidden and is noticeable for large Δ. On the other hand, a small Δ is better for carrier separation in momentum space to suppress the radiative recombination. Electronic band structure of $CsCu_5Se_3$ in Figure 6d is very similar to that of the former $CsCu_5S_3$ semiconductor. The indirect band gap and direct band gap differ by 33 meV in $CsCu_5Se_3$. However, along with the small energy differences between direct and indirect band gaps, there are flat bands near the VBM of $CsCu_5X_3$ (see Figures 6c and d), which are related to the layered electronic structures, as shown in Figures 6e and f, illustrating that the charge density are mainly located on the Cu-X layers and are separated by the Cs^+ ions. This type of electronic structure was found in hybrid perovskite solar cell materials.[34] Figure S2 shows that the charge density of $CsPbI_3$ also shares the common features of covalent framework and isolated ions. Moreover, the mixed covalent–ionic electronic structure is very different from that of the traditional PV materials (such as Si, CdTe, $CuIn_xGa_{(1-x)}Se_2$, and Cu_2ZnSnS_4).

Theoretical Prediction. The successful synthesis of $CsCu_5S_3$ and $CsCu_5Se_3$ suggests that $CsCu_5Te_3$ could be a missing stable compound. Similar compound $CsAg_5Te_3$ was previously described as having good thermoelectrics.[35] The calculated total energies of $CsCu_5S_3$- and $CsAg_5Te_3$-structure types of hypothesized $CsCu_5Te_3$ were compared, and the $CsCu_5S_3$-type was shown to exhibit the lowest energy. The $CsCu_5Te_3$ was also shown to be stable with respect to its competing phases via chemical potential space analysis (Figure 7a). Its stability region (in green) is located near the Cu-poor Cs-rich corner. Figure 7b shows the electronic structure of $CsCu_5Te_3$. The valence bands are analogous to those of $CsCu_5S_3$ and $CsCu_5Se_3$; the VBM is at Z point, which is slightly
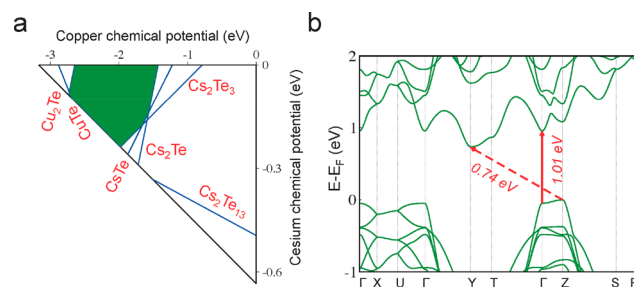
Figure 7. (a) Stability analysis in the chemical potential space of $CsCu_5Te_3$. (b) Electronic band structures of $CsCu_5Te_3$ from DFT with band gap corrected by HSE06.

higher than the first valence state at Γ. While the conduction bands in $CsCu_5Te_3$ are different compared to those in $CsCu_5S_3$ and $CsCu_5Se_3$, the first conduction band at Y point drops and becomes the CBM. Furthermore, the electron effective mass of $CsCu_5Te_3$ is quite different from those of $CsCu_5S_3$ and $CsCu_5Se_3$ (see Table 3). The hole effective masses of $CsCu_5X_3$

Table 3. Calculated Effective Masses of $CsCu_5X_3$ (X = S, Se, Te)

compound	space group	electron effective mass $(m_{xx}^e, m_{yy}^e, m_{zz}^e)$	hole effective mass $(m_{xx}^h, m_{yy}^h, m_{zz}^h)$
$CsCu_5S_3$	$Pmma$	(0.34, 0.33, 0.32)	(5.78, 0.21, 13.36)
$CsCu_5Se_3$	$Pmma$	(0.19, 0.09, 0.21)	(4.29, 0.14, 5.67)
$CsCu_5Te_3$	$Pmma$	(0.16, 0.30, 2.77)	(2.19, 0.09, 3.54)

are all highly anisotropic, the effective mass along z direction (see the flat band along Γ−Z) is very large; however, the effective mass along y direction is very small. Therefore, when the material is p-type doped, the holes can transport along the y-axis.

CONCLUSION

In summary, the new semiconductor $CsCu_5Se_3$ isostructural to $CsCu_5S_3$ was successfully synthesized in good yield, and the stability of $CsCu_5Te_3$ was predicted. The nearly direct band gaps of $CsCu_5X_3$ (X = S, Se) calculated with the hybrid DFT close to 1.4 eV were further confirmed by optical absorption spectroscopy, and band structures of $CsCu_5Te_3$ were also predicted. This type of band structure is desirable for optoelectronic applications because it suppresses radiative recombination of photogenerated carriers with very low energy loss. This combined theory−experiment approach is a major step toward discovery of new chalcogenide semiconductor materials for optoelectronic applications.

ASSOCIATED CONTENT

Ⓢ Supporting Information

The Supporting Information is available free of charge on the ACS Publications website at DOI: 10.1021/acs.chemmater.7b05104.

> EDX analysis and comparison of the band structure and charge density of $CsPbI_3$ from DFT (PDF)
> Crystallographic information for $CsCu_5S_3$ (CIF)
> Crystallographic information for $CsCu_5Se_3$ (CIF)

AUTHOR INFORMATION

Corresponding Authors
*E-mail: xiazg@ustb.edu.cn.
*E-mail: xiuwenzhang@szu.edu.cn.
*E-mail: krp@northwestern.edu.

ORCID Ⓞ
Zhiguo Xia: 0000-0002-9670-3223
Romain Gautier: 0000-0002-3042-0335
Qingfeng Yan: 0000-0002-5084-6886
Kenneth R. Poeppelmeier: 0000-0003-1655-9127

Author Contributions
△Z.X. and H.F. contributed equally.

Notes
The authors declare no competing financial interest.

REFERENCES

(1) Gautier, R.; Zhang, X.; Hu, L.; Yu, L.; Lin, Y.; Sunde, T. O.; Chon, D.; Poeppelmeier, K. R.; Zunger, A. Prediction and accelerated laboratory discovery of previously unknown 18-electron ABX compounds. *Nat. Chem.* **2015**, *7*, 308−316.

(2) Hautier, G.; Fischer, C.; Ehrlacher, V.; Jain, A.; Ceder, G. Data mined ionic substitutions for the discovery of new compounds. *Inorg. Chem.* **2011**, *50*, 656−663.

(3) Wu, K.; Yang, Z.; Pan, S. Na_2BaMQ_4 (M = Ge, Sn; Q = S, Se): Infrared Nonlinear Optical Materials with Excellent Performances and that Undergo Structural Transformations. *Angew. Chem., Int. Ed.* **2016**, *55*, 6713−6715.

(4) Wu, K.; Zhang, B.; Yang, Z.; Pan, S. New Compressed Chalcopyrite-like $Li_2BaMIVQ_4$ (MIV = Ge, Sn; Q = S, Se): Promising Infrared Nonlinear Optical Materials. *J. Am. Chem. Soc.* **2017**, *139*, 14885−14888.

(5) Curtarolo, S.; Hart, G. L.; Nardelli, M. B.; Mingo, N.; Sanvito, S.; Levy, O. The high-throughput highway to computational materials design. *Nat. Mater.* **2013**, *12*, 191−201.

(6) Hu, S.; Shaner, M. R.; Beardslee, J. A.; Lichterman, M.; Brunschwig, B. S.; Lewis, N. S. Amorphous TiO_2 coatings stabilize Si, GaAs, and GaP photoanodes for efficient water oxidation. *Science* **2014**, *344*, 1005−1009.

(7) Saldanha, P. L.; Brescia, R.; Prato, M.; Li, H.; Povia, M.; Manna, L.; Lesnyak, V. Generalized One-Pot Synthesis of Copper Sulfide, Selenide-Sulfide, and Telluride-Sulfide Nanoparticles. *Chem. Mater.* **2014**, *26*, 1442−1449.

(8) Kriegel, I.; Jiang, C.; Rodríguez-Fernández, J.; Schaller, R. D.; Talapin, D. V.; Da Como, E.; Feldmann, J. Tuning the Excitonic and Plasmonic Properties of Copper Chalcogenide Nanocrystals. *J. Am. Chem. Soc.* **2012**, *134*, 1583−1590.

(9) Wu, L.; Chen, S.-Y.; Fan, F.-J.; Zhuang, T.-T.; Dai, C.-M.; Yu, S.-H. Polytypic Nanocrystals of Cu-based Ternary Chalcogenides: Colloidal Synthesis and Photoelectrochemical Properties. *J. Am. Chem. Soc.* **2016**, *138*, 5576−5584.

(10) Zhang, X.; Yu, L.; Zakutayev, A.; Zunger, A. Sorting Stable versus Unstable Hypothetical Compounds: The Case of Multi-Functional ABX Half-Heusler Filled Tetrahedral Structures. *Adv. Funct. Mater.* **2012**, *22*, 1425−1435.

(11) Vermeer, M. J. D.; Zhang, X.; Trimarchi, G.; Donakowski, M. D.; Chupas, P. J.; Poeppelmeier, K. R.; Zunger, A. Prediction and Synthesis of Strain Tolerant RbCuTe Crystals Based on Rotation of One-Dimensional Nano Ribbons within a Three-Dimensional Inorganic Network. *J. Am. Chem. Soc.* **2015**, *137*, 11383−11390.

(12) Savelsberg, G.; Schäfer, H. On Ternary Pnictides and Chalcogenides of Alkaline Metals and IB- resp. II B-Elements. *Z. Naturforsch.* **1978**, *33b*, 370−373.

(13) Powell, A. E.; Hodges, J. M.; Schaak, R. E. Preserving Both Anion and Cation Sublattice Features during a Nanocrystal Cation Exchange Reaction: Synthesis of Metastable Wurtzite-Type CoS and MnS. *J. Am. Chem. Soc.* **2016**, *138*, 471−474.

(14) Xuan, T.; Yang, X.; Lou, S.; Huang, J.; Liu, Y.; Yu, J.; Li, H.; Wong, K.; Wang, C.; Wang, J. *Nanoscale* **2017**, *9*, 15286−15290.

(15) Effenberger, H.; Pertlik, F. Crystal structure of $NaCu_5S_3$. *Monatsh. Chem.* **1985**, *116*, 921−926.

(16) Dai, S.; Xi, Y.; Hu, C.; Liu, J.; Zhang, K.; Yue, X.; Cheng, L. KCu_7S_4 nanowires and the Mn/KCu_7S_4 nanostructure for solid-state supercapacitors. *J. Mater. Chem. A* **2013**, *1*, 15530−15534.

(17) Harrison, W. T. A.; Nenoff, T. M.; Gier, T. E.; Stucky, G. D. Tetrahedral-atom 3-ring groupings in 1-dimensional inorganic chains: $Be_2AsO_4OH\bullet4H_2O$ and $Na_2ZnPO_4OH\bullet7H_2O$. *Inorg. Chem.* **1993**, *32*, 2437−2441.

(18) Kohn, W.; Sham, L. J. Self-Consistent Equations Including Exchange and Correlation Effects. *Phys. Rev.* **1965**, *140*, A1133−A1138.

(19) Kresse, G.; Joubert, D. From ultrasoft pseudopotentials to the projector augmented-wave method. *Phys. Rev. B: Condens. Matter Mater. Phys.* **1999**, *59*, 1758−1775.

(20) Perdew, J. P.; Burke, K.; Ernzerhof, M. Generalized Gradient Approximation Made Simple. *Phys. Rev. Lett.* **1996**, *77*, 3865−3868.

(21) Kresse, G.; Furthmüller, J. Efficiency of ab-initio total energy calculations for metals and semiconductors using a plane-wave basis set. *Comput. Mater. Sci.* **1996**, *6*, 15−50.

(22) Błoński, P.; Hafner, J. Magnetic anisotropy of transition-metal dimers: Density functional calculations. *Phys. Rev. B: Condens. Matter Mater. Phys.* **2009**, *79*, 224418.

(23) Heyd, J.; Scuseria, G. E.; Ernzerhof, M. Erratum. Hybrid functionals based on a screened Coulomb potential. *J. Chem. Phys.* **2003**, *118*, 8207−8215.

(24) Huster, J.; Bronger, W. $CsCu_5S_3$−eine neue Verbindung in zwei Modifikationen. *Z. Anorg. Allg. Chem.* **2001**, *627*, 1395−1400.

(25) Kokh, K.; Atuchin, V.; Gavrilova, T.; Kuratieva, N.; Pervukhina, N.; Surovtsev, N. *Solid State Commun.* **2014**, *177*, 16−19.

(26) Atuchin, V.; Borisov, S.; Gavrilova, T.; Kokh, K.; Kuratieva, N.; Pervukhina, N. *Particuology* **2016**, *26*, 118−122.

(27) Mott, D.; Yin, J.; Engelhard, M.; Loukrakpam, R.; Chang, P.; Miller, G.; Bae, I.-T.; Chandra Das, N.; Wang, C.; Luo, J. From Ultrafine Thiolate-Capped Copper Nanoclusters toward Copper Sulfide Nanodiscs: A Thermally Activated Evolution Route. *Chem. Mater.* **2010**, *22*, 261−271.

(28) Majeski, M. W.; Bolotin, I. L.; Hanley, L. Cluster Beam Deposition of $Cu_{2−x}S$ Nanoparticles into Organic Thin Films. *ACS Appl. Mater. Interfaces* **2014**, *6*, 12901−12908.

(29) Atuchin, V.; Isaenko, L.; Kesler, V.; Lobanov, S. *J. Alloys Compd.* **2010**, *497*, 244−248.

(30) Dolgonos, A.; Mason, T. O.; Poeppelmeier, K. R. Direct optical band gap measurement in polycrystalline semiconductors: A critical look at the Tauc method. *J. Solid State Chem.* **2016**, *240*, 43−48.

(31) Liang, D.; Kang, Y.; Huo, Y.; Chen, Y.; Cui, Y.; Harris, J. S. High-efficiency nanostructured window GaAs solar cells. *Nano Lett.* **2013**, *13*, 4850−4856.

(32) Kaur, J.; Bethge, O.; Wibowo, R. A.; Bansal, N.; Bauch, M.; Hamid, R.; Bertagnolli, E.; Dimopoulos, T. All-oxide solar cells based on electrodeposited Cu_2O absorber and atomic layer deposited ZnMgO on precious-metal-free electrode. *Sol. Energy Mater. Sol. Cells* **2017**, *161*, 449−459.

(33) Yu, L.; Zunger, A. Identification of potential photovoltaic absorbers based on first-principles spectroscopic screening of materials. *Phys. Rev. Lett.* **2012**, *108*, 068701.

(34) Yin, W.; Shi, T.; Yan, Y. Unusual defect physics in $CH_3NH_3PbI_3$ perovskite solar cell absorber. *Appl. Phys. Lett.* **2014**, *104*, 063903.

(35) Lin, H.; Tan, G.; Shen, J. N.; Hao, S.; Wu, L. M.; Calta, N.; Malliakas, C.; Wang, S.; Uher, C.; Wolverton, C. Concerted Rattling in $CsAg_5Te_3$ Leading to Ultralow Thermal Conductivity and High Thermoelectric Performance. *Angew. Chem., Int. Ed.* **2016**, *55*, 11431−11436.